Ukrainian Journal of Physical Optics
ISSUE 2
2026

GENERATION OF THE TOPOLOGICAL DIPOLES OF THE ORIENTATION OF OPTICAL INDICATRIX AND OPTICAL VORTICES BY THE BENDING STRESS IN POLYCARBONATE BAR

O. KRUPYCH, D. ADAMENKO, T. DUDOK, I. SKAB, R. VLOKH *

O.G.Vlokh Institute of Physical Optics of the Ivan Franko National University of Lviv,
23 Dragomanov Str., 79005, Lviv, Ukraine
*Corresponding author: vlokh@ifo.lviv.ua

Received: 24.02.2026

Abstract. The topological defects of the optical indicatrix orientation in a polycarbonate bar subjected to bending stress caused by distributed loading were experimentally revealed. It has been found that topological defects (TDs) are paired as topological dipoles, consisting of defects with the same half-integer strength but opposite signs. These TDs produce single-charged optical vortices with opposite orbital angular momentum (OAM) signs when circularly polarized light is incident on the polycarbonate bar. It has been shown that the sign of the OAM of the outgoing beam is positive when the signs of the TD's strength and spin angular momentum (SAM_{in}) of the incident photons are the same, and negative when the signs of the TD's strength and SAM_{in} of the incident photons are different. Therefore, the sign of TD strength and SAM_{in} yields the sign of OAM, so that the media acts on the angular momentum like an XNOR logical gate. At the same time, the signs of incident and outgoing SAMs are always opposite, which relates to the NOT logical gate.

Keywords: topological defects, optical vortex, optical indicatrix, polarization singularities, bending stress, polycarbonate
UDC: 535.5
DOI: 10.3116/16091833/Ukr.J.Phys.Opt.2026.02070

1. Introduction

Topological defects (TDs) are significant across various physics disciplines, including condensed matter physics, quantum physics, optics, and cosmology [1-8]. Some cosmological models suggest that monopoles, strings, membranes, and textures emerge as the early Universe cools [9]. These represent specific TDs of different dimensions. The formation of structural defects in solid materials and liquid crystals (LC) [10-12] is linked to symmetry-breaking during phase transitions, with TDs located at the sites where a low-symmetry phase nucleates [13]. In optics, defects in LC directors can produce optical vortices (OV) carrying nonzero orbital angular momentum [14], crucial for quantum computing [15,16], entanglement, teleportation [17-20], microparticle control [21], and super-resolution imaging For the generation of OVs using LC, *q*-plates have been proposed [22], which, in fact, represent LC cells with TDs of director orientation. In the simplest case, the topological strength of such TD is equal to unity. The process of transforming a circularly polarized optical wave into a vortex-bearing wave has been called spin angular momentum-to-orbit angular momentum (SAM-to-OAM) conversion [23]. This process suggests that the incident optical beam's SAM is converted into the OAM of the beam emerging from the *q*-plate. However, as assumed in [25,25] such a description can be applied only to the axially symmetric director distribution around the TD of *q*-plates. In fact, for the strength of TDs

greater then unity the conservation law of the optical angular momentum is not satisfied, while for the strength of defect equal to $\pm n/2$ (n=1,3,5…) one should assume the transformation of the part of the angular momentum to the mechanical angular momentum of the media. It should be noted that not only the sign of the SAM_{in} of the incident beam has to play the role in the sign of the OAM of the generated vortex beam, but, as it will be shown below, the sign of the strength of TD also. By making this work, we had the possibility to generate defects with half-integer strength and of both signs in a single medium and to control the sign of the generated OVs.

2. Experimental method

Recently, we experimentally observed TDs in the orientation of the optical indicatrix (OI) induced by conical electric fields [26-28], torsion and bending strains [29-31], and residual stresses in glasses [32,33]. Bending a bar is one of the simplest from the point of view of experimental implementation, since in this case any medium, even isotropic glass, can be used. Moreover, it is not necessary to make predisposal orientation of samples. In addition, the parameters of the applied bending stress can be chosen in such a way that the generated optical vortex is close to isotropic [34]. To induce bending stress distributed over a specific distance on the top surface of the transparent bar, we used the sample-loading scheme shown in Fig. 1. The polycarbonate (PC) has been used since this material possess extremely high values of piezo-optic coefficients, i.e., $\pi_{66}=-39.2\times10^{-12}$ m^2/N, $\pi_{11}=-4.6\times10^{-12}$ m^2/N $\pi_{12}=34.6\times10^{-12}$ m^2/N [35] and is suitable for optical vortices generation with bending method [36]. The parameters of the PC bar and the experimental setup (Fig. 1) were $2h$=13.8 mm, d=15.3 mm, $2b$=4.5 mm, and $2l$=36.0 mm.

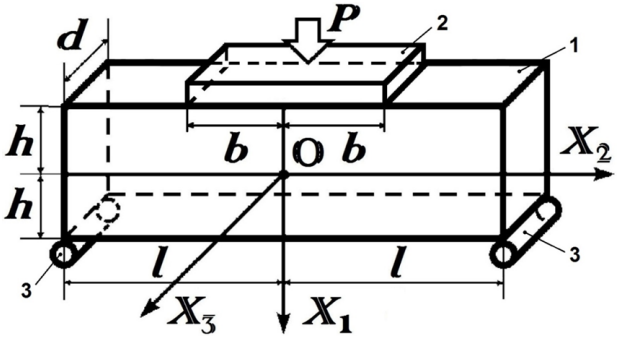

Fig. 1. Scheme of applying load P distributed over the distance $2b$ on the upper surface of a sample in the shape of a rectangular bar: 1 – sample; 2 – punch; 3 – supports.

The optical retardation and the azimuthal orientation of the polarization ellipse of the light beam exiting the sample have been studied using an imaging polarimeter described in detail in our work [37]. For the obtaining of the orientation of the axis of the optical indicatrix, one has to add 45 deg to the azimuthal orientation of the polarization ellipse. The interference patterns were obtained using a Mach-Zehnder interferometer, in which the sample loaded by the bending stress was placed in the probe arm. At the same time, the reference arm contained a long-focus lens for the creation of the spherical wavefront. As the light source, a He-Ne laser (λ = 632.8 nm) has been used. The wide optical beam with a diameter of 20 mm has been propagated along the positive direction of the X_3 axis (Fig. 1). The tracing angle (φ) was counted from the positive direction of the X_1 axis toward the positive X_2 axis.

3. Results and discussion

Fig. 2 shows the maps of retardation (Fig. 2a) and the orientation of the principal axis of OI (Fig. 2b) for the sample free from a bent load. It is observed that near the upper and lower surfaces of the sample, the retardation reaches about 90 deg, while the angle of OI orientation is about 130 deg. In the central part of the sample, these parameters are close to 30 and 60 deg, respectively. It is clear that the nonzero retardation and specific angle of OI orientation are caused by residual stresses present in the polycarbonate sample. A nonzero angle of OI orientation indicates that the shear stress σ_6 is present among the components of the residual stress tensor. Assuming that the residual stress possesses a 2D configuration and does not depend on the X_3 axis, one can determine the residual birefringence as $\Delta n = \lambda\Delta\phi / 2\pi d$ ($\Delta\phi$ - is the retardation and Δn - birefringence). By neglecting the π_{11} piezo-optic coefficient, which is significantly smaller than π_{12} and π_{66}, the equation for the OI cross-section in the X_1X_2 plane under residual stress components σ_2 and σ_6 can be expressed as:

$$(B_{11} + \pi_{12}\sigma_2)X_1^2 + B_{11}X_2^2 + 2\pi_{66}\sigma_6 X_1^2 X_2^2 = 1\,, \tag{1}$$

where B_{11} is the component of the dielectric impermeability tensor. Then the birefringence (Δn) and the angle of OI rotation (ζ) can be defined as:

$$\Delta n = \frac{1}{2} n^3 \sqrt{\pi_{12}^2\sigma_2^2 + 4\pi_{66}^2\sigma_6^2}\,, \tag{2}$$

$$\tan 2\zeta = \frac{2\pi_{66}\sigma_6}{\pi_{12}\sigma_2}\,. \tag{3}$$

where $n = 1.5816$ is the refractive index at λ=632.8 nm [35]. Then, by solving the system of Eq. (2,3), one can determine the components of the stress tensor as:

$$\sigma_2 = \frac{2\Delta n \cos 2\zeta}{n^3\pi_{12}}\,, \tag{4}$$

$$\sigma_6 = \frac{\pi_{12}\sigma_2 \tan 2\zeta}{2\pi_{66}}\,. \tag{5}$$

It has been found that their values are about $\sigma_2 = 4.3\times10^4$ N/m^2 and $\sigma_6 = -1.1\times10^4$ N/m^2 in the

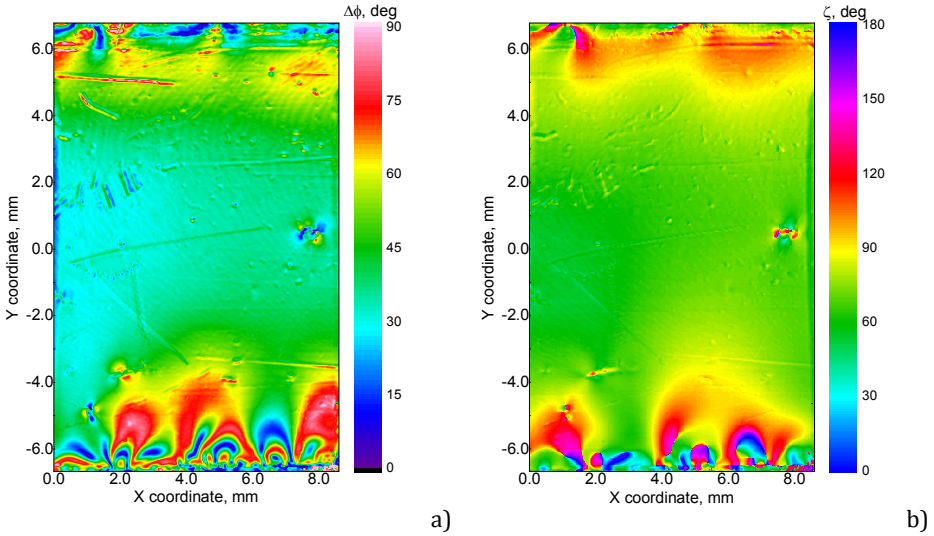

a) b)

Fig. 2. The maps of retardation (a) and orientation of the principal axis of the OI (b) of the polycarbonate sample without applied bending stress.

central part of the sample, and σ_2=1.5×10^5 N/m^2 and σ_6=1.1×10^4 N/m^2 near the edge parts of the sample. Notice that the applied load is P=137 N, corresponding to an external stress of 2×10^{6}N/m^2. Therefore, the applied stress is about an order of magnitude higher than the residual one.

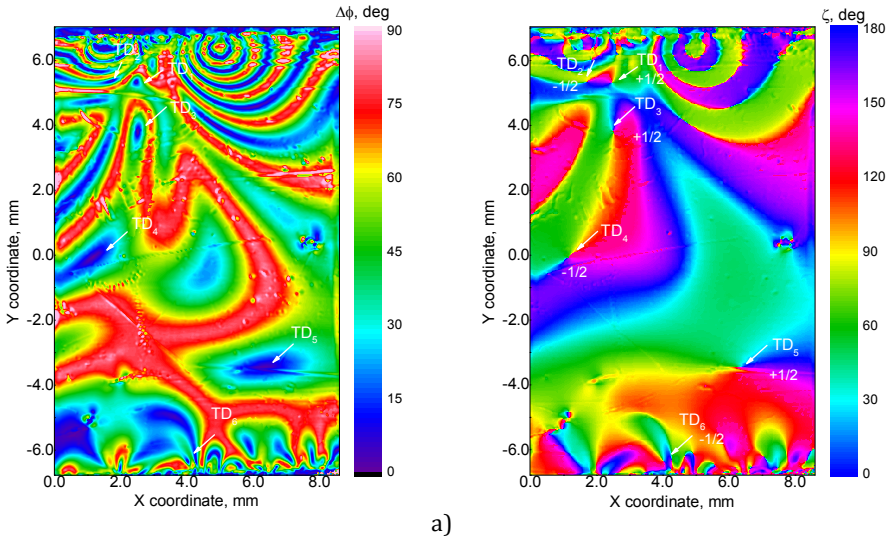

a) b)

Fig. 3. The maps of retardation (a) and orientation of the principal axis of the OI (b) of the polycarbonate sample under applied bending stress with 137 N loading.

Fig. 3 shows maps of retardation and the orientation of the principal axis of the OI under a bending load of 137 N. As observed, at least six TDs (TD_1-TD_6) are clearly visible. At the locations of these TDs, the retardation is zero, and the orientation of the OI's principal axis is undefined. Three pairs of these defects – specifically TD_1 and TD_2, TD_3 and TD_4, and TD_5 and TD_6 – form topological dipoles by defects of opposite strengths. The opposite signs of defects strength correspond to lemon (+1/2) and star (–1/2) defects (Fig. 4). The appearance of six TDs of OI orientation, instead of one predicted by the theory for the case of bending under a distributed load [29] and demonstrated experimentally on a glass bar [34], can be explained by the high piezo-optic figure of merit of polycarbonate and its sensitivity to misalignment of stress application, as well as the presence of residual stress and birefringence in the sample.

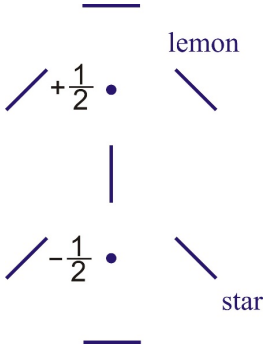

Fig. 4. Topological dipole created by lemon and star TDs. The line segments indicate the orientation of the OI axis.

Fig. 5 shows the detected spiral interference patterns originating from TD_1 and TD_2 defects. Since the spiral-like patterns possess a single fringe, the generated vortices are single-charged. It is seen that the spiral-like patterns have opposite handedness. Therefore, the single-charged OVs generated by these TDs have opposite OAM signs, despite the

incident circularly polarized optical beam having the same handedness for the case of both TDs. Therefore, the sign of the generated OV charge depends not only on the sign of SAM_{in} but also on the sign of TD.

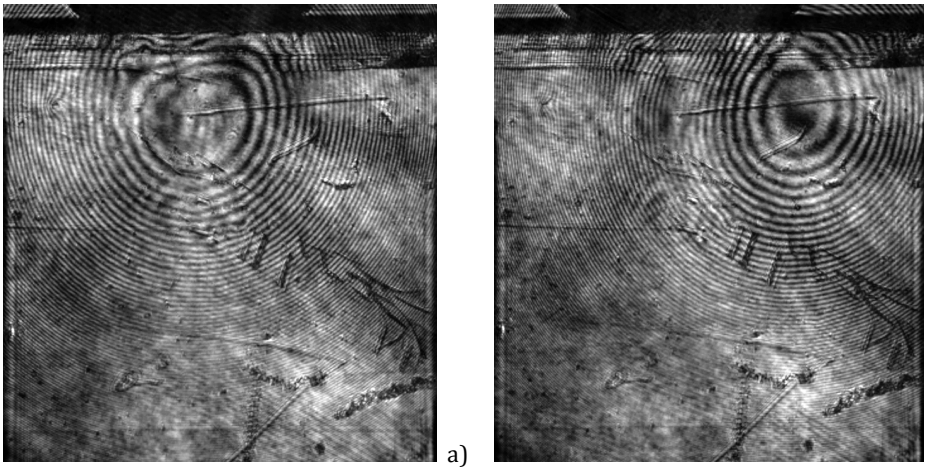

a) (b)

Fig. 5. Spiral-like interference of the vortex beam with a Gaussian spherical beam. (a) OV is caused by TD_1; (b) OV is caused by TD_2.

Let us consider the relations describing the generated OVs by TDs. In the case of right handed incident optical wave and positive strength of TD, the electric field of the outgoing optical wave can be written as:

$$E_{out} = M(q)\begin{pmatrix}1\\ i\end{pmatrix} = \begin{pmatrix}\cos 2q\varphi & \sin 2q\varphi\\ \sin 2q\varphi & -\cos 2q\varphi\end{pmatrix}\begin{pmatrix}1\\ i\end{pmatrix} = e^{i2q\varphi}\begin{pmatrix}1\\ -i\end{pmatrix}, \tag{6}$$

where $M(q) = \begin{pmatrix}\cos 2q\varphi & \sin 2q\varphi\\ \sin 2q\varphi & -\cos 2q\varphi\end{pmatrix}$ is the Jones matrix of the Pancharatnam-Berry phase optical element [24], q – is the strength of TD. As can be seen, the outgoing left-handed circularly polarized optical wave carries OAM $l = 2q = 1$. In the case when the strength of TD is negative, the electric field of the outgoing optical wave is written as:

$$E_{out} = M(-q)\begin{pmatrix}1\\ i\end{pmatrix} = \begin{pmatrix}\cos 2q\varphi & -\sin 2q\varphi\\ -\sin 2q\varphi & -\cos 2q\varphi\end{pmatrix}\begin{pmatrix}1\\ i\end{pmatrix} = e^{-i2q\varphi}\begin{pmatrix}1\\ -i\end{pmatrix}. \tag{7}$$

Therefore, the outgoing circular wave possesses left-handed circular polarization, and the OAM is equal to $l = -2q = -1$. If the incident optical wave is left-handed, the respective relations are as follows:

$$E_{out} = M(q)\begin{pmatrix}1\\ -i\end{pmatrix} = \begin{pmatrix}\cos 2q\varphi & \sin 2q\varphi\\ \sin 2q\varphi & -\cos 2q\varphi\end{pmatrix}\begin{pmatrix}1\\ -i\end{pmatrix} = e^{-i2q\varphi}\begin{pmatrix}1\\ i\end{pmatrix}, \tag{8}$$

i.e., the right-handed circular optical wave bears OV with negative charge $l = -2q = -1$, and

$$E_{out} = M(-q)\begin{pmatrix}1\\ -i\end{pmatrix} = \begin{pmatrix}\cos 2q\varphi & -\sin 2q\varphi\\ -\sin 2q\varphi & -\cos 2q\varphi\end{pmatrix}\begin{pmatrix}1\\ -i\end{pmatrix} = e^{i2q\varphi}\begin{pmatrix}1\\ i\end{pmatrix}. \tag{9}$$

The right-handed outgoing circular wave bears OV with a positive charge $l = 2q = 1$. Notice that relations (6-9) are written for the conditions that the retardation is equal to λ/2, i.e., all the intensity of the incident optical beam is transformed to the outgoing vortex beam. From

the above formulas, it is seen that in the case of positive strength of TD, the sign of OAM is determined by the handedness of the incident optical wave, i.e., the sign of SAM_{in}. However, it is not so in the case of a negative sign of TD strength. When the SAM_{in} of incident photons is positive, the left-handed outgoing wave carries OAM with a negative sign, determined by the sign of the TD strength. When both the SAM_{in} of incident photons and the sign of TD strength are negative, the right-handed outgoing beam bears OV with positive charge. Therefore, both the sign of the SAM_{in} of the incident photons, and the sign of the TD strength determine the sign of the OV charge (Table 1). In our experiment, we deal with TDs of opposite sign, while the SAM_{in} sign of the incident photons remains unchanged. Following from the above relations, the sign of the OV charge is determined only by the sign of the TD's strength in this case. Thus, we have experimentally proved this property.

Table 1. Change of OAM in dependence on TD sign and SAM_{in}.

№ of equation	TD sign	SAM_{in} sign	OAM sign	SAM_{out} sign
6	+	+	+	–
8	+	–	–	+
7	–	+	–	–
9	–	–	+	+

It is seen (Table 1) that the sign of TD strength and SAM_{in} results in the sign of OAM, such that the media acts on the angular momentum like an XNOR logical gate. It means that when TD and SAM_{in} signs are the same, the sign of OAM is positive, whereas when they differ, the sign of OAM is negative. At the same time, the signs of incident and outgoing SAMs are always opposite, which corresponds to the NOT logical gate.

4. Conclusions

In the present study, we experimentally revealed the TDs of the optical indicatrix orientation in a polycarbonate bar subjected to bending stress induced by distributed loading. It has been found that TDs pairs create topological dipoles consisting of defects of half-integer strength, but with opposite signs. These TDs generate the single-charged OVs with opposite sign when circularly polarized light is incident on the polycarbonate bar. It has been shown that in the two cases when the SAM of the incident photons is the same in sign, the sign of the OAM of the outgoing beam depends on the sign of the TD's strength. In other words, the sign of the OAM of the outgoing beam is positive when the signs of the TD's strength and SAM_{in} of the incident photons are the same, and negative when the signs of the TD's strength and SAM_{in} of the incident photons are different. Therefore, the sign of TD strength and SAM_{in} results in the sign of OAM, such that the media acts on the angular momentum like an XNOR logical gate. At the same time, the signs of incident and outgoing SAMs are always opposite, which relates to the NOT logical gate.

Funding. The present work is supported by the Ministry of Education and Science of Ukraine (project # 0124U000979).

Conflict of interest. Authors declare no conflict of interest.

References

1. Seidel, J. (2016). Topological structures in ferroic materials. *Switzerland: Springer International Publishing*, *228*.
2. Nagali, E., Sciarrino, F., De Martini, F., Marrucci, L., Piccirillo, B., Karimi, E., & Santamato, E. (2009). Quantum information transfer from spin to orbital angular momentum of photons. *Physical Review Letters*, *103*(1), 013601.
3. Salomaa, M. M., & Volovik, G. E. (1987). Quantized vortices in superfluid ^{3}He. *Reviews of Modern Physics*, *59*(3), 533.

4. Onsager, L. (1949). The two fluid model for helium II [remarks by L. Onsager on pp. 249–250]. *Nuovo Cimento Suppl*, *6*, 249-250.
5. Zurek, W. H. (1985). Cosmological experiments in superfluid helium?. *Nature*, *317*(6037), 505-508.
6. Trebin, H. R. (1998). Defects in liquid crystals and cosmology. *Liquid Crystals*, *24*(1), 127-130.
7. Kibble, T. W. (1976). Topology of cosmic domains and strings. *Journal of Physics A: Mathematical and General*, *9*(8), 1387-1398.
8. Lin, S. Z., Wang, X., Kamiya, Y., Chern, G. W., Fan, F., Fan, D., Casas, B., Liu, Y., Kiryukhin, V., Zurek, W. H.C., Batista, D. & Cheong, S. W. (2014). Topological defects as relics of emergent continuous symmetry and Higgs condensation of disorder in ferroelectrics. *Nature Physics*, *10*(12), 970-977.
9. Vilenkin, A., Vilenkin, A., & Shellard, E. P. S. (1994). *Cosmic strings and other topological defects*. Cambridge University Press.
10. Kurik, M. V., & Lavrentovich, O. D. (1988). Defects in liquid crystals: homotopy theory and experimental studies. *Soviet Physics Uspekhi*, *31*(3), 196-224.
11. Mermin, N. D. (1979). The topological theory of defects in ordered media. *Reviews of Modern Physics*, *51*(3), 591.
12. Kleman, M., & Lavrentovich, O. D. (2006). Topological point defects in nematic liquid crystals. *Philosophical Magazine*, *86*(25-26), 4117-4137.
13. Boulbitch, A. A., & Toledano, P. (1998). Phase nucleation of elastic defects in crystals undergoing a phase transition. *Physical Review Letters*, *81*(4), 838.
14. Marrucci, L., Karimi, E., Slussarenko, S., Piccirillo, B., Santamato, E., Nagali, E., & Sciarrino, F. (2011). Spin-to-orbital conversion of the angular momentum of light and its classical and quantum applications. *Journal of Optics*, *13*(6), 064001.
15. Nielsen, M. A., & Chuang, I. L. (2010). *Quantum computation and quantum information*. Cambridge university press.
16. Molina-Terriza, G., Torres, J. P., & Torner, L. (2001). Management of the angular momentum of light: preparation of photons in multidimensional vector states of angular momentum. *Physical Review Letters*, *88*(1), 013601.
17. Chen, L., & She, W. (2008). Electro-optically forbidden or enhanced spin-to-orbital angular momentum conversion in a focused light beam. *Optics Letters*, *33*(7), 696-698.
18. Li, P., Sun, Y., Yang, Z., Song, X., & Zhang, X. (2015). Classical hypercorrelation and wave-optics analogy of quantum superdense coding. *Scientific Reports*, *5*(1), 18574.
19. D'Ambrosio, V., Carvacho, G., Graffitti, F., Vitelli, C., Piccirillo, B., Marrucci, L., & Sciarrino, F. (2016). Entangled vector vortex beams. *Physical Review A*, *94*(3), 030304.
20. Chen, L., & She, W. (2009). Teleportation of a controllable orbital angular momentum generator. *Physical Review A – Atomic, Molecular, and Optical Physics*, *80*(6), 063831.
21. Gahagan, K. T., & Swartzlander Jr, G. A. (1996). Optical vortex trapping of particles. *Optics Letters*, *21*(11), 827-829.
22. Rubano, A., Cardano, F., Piccirillo, B., & Marrucci, L. (2019). Q-plate technology: a progress review. *Journal of the optical society of america B*, *36*(5), D70-D87.
23. Marrucci, L., Manzo, C., & Paparo, D. (2006). Optical spin-to-orbital angular momentum conversion in inhomogeneous anisotropic media. *Physical Review Letters*, *96*(16), 163905.
24. Marrucci, L. (2007, May). Rotating light with light: Generation of helical modes of light by spin-to-orbital angular momentum conversion in inhomogeneous liquid crystals. In *Liquid crystals and applications in optics* (Vol. 6587, pp. 56-66). SPIE.
25. Bliokh, K. Y., Rodríguez-Fortuño, F. J., Nori, F., & Zayats, A. V. (2015). Spin–orbit interactions of light. *Nature Photonics*, *9*(12), 796-808.
26. Skab, I., Vasylkiv, Y., Smaga, I., & Vlokh, R. (2011). Spin-to-orbital momentum conversion via electro-optic Pockels effect in crystals. *Physical Review A – Atomic, Molecular, and Optical Physics*, *84*(4), 043815.
27. Vasylkiv, Y., Skab, I., & Vlokh, R. (2014). Generation of double-charged optical vortices on the basis of electro-optic Kerr effect. *Applied Optics*, *53*(10), B60-B73.
28. Vasylkiv, Y., Krupych, O., Skab, I., & Vlokh, R. (2011). On the spin-to-orbit momentum conversion operated by electric field in optically active $Bi_{12}GeO_{20}$ crystals. *Ukrainian Journal of Physical Optics*, *12*(4), 171-179.
29. Skab, I., Vasylkiv, Y., & Vlokh, R. (2012). Induction of optical vortex in the crystals subjected to bending stresses. *Applied Optics*, *51*(24), 5797-5805.
30. Skab, I., Vasylkiv, Y., Zapeka, B., Savaryn, V., & Vlokh, R. (2011). Appearance of singularities of optical fields under torsion of crystals containing threefold symmetry axes. *Journal of the Optical Society of America A*, *28*(7), 1331-1340.
31. Skab, I., Vasylkiv, Y., Savaryn, V., & Vlokh, R. (2011). Optical anisotropy induced by torsion stresses in LiNbO 3 crystals: appearance of an optical vortex. *Journal of the Optical Society of America A*, *28*(4), 633-640.
32. Vasylkiv, Y., Kryvyy, T., Skab, I., & Vlokh, R. (2016). Conditions of appearance of the topological defects of optical indicatrix orientation in the glasses with residual stresses: Movement of the defects under application of external mechanical stress to CaB_4O_7 glasses. *Ukrainian Journal of Physical Optics*, *17* (2), 65-74.
33. Vasylkiv, Y., Skab, I., & Vlokh, R. (2016). Identification of the topological defects of optical indicatrix orientation in CaB_4O_7 glasses. *Journal of Optics*, *18*(8), 084006.

34. Krupych, O., Adamenko, D., Dudok, T., Skab, I., & Vlokh, R. (2026). Optical vortex generation using a glass plate bent by a load distributed over a finite distance. *Ukrainian Journal of Physical Optics*, *27*(1), 01102-01109.
35. Waxler, R. M., Horowitz, D., & Feldman, A. (1979). Optical and physical parameters of Plexiglas 55 and Lexan. *Applied Optics*, *18*(1), 101-104.
36. Vasylkiv, Y., Smaga, I., Skab, I., & Vlokh, R. (2013). Efficient materials for spin-to-orbit angular momentum conversion using bending technique. *Ukrainian Journal of Physical Optics*, *14* (4), 200-209.
37. Krupych, O., Dudok, T., Skab, I., Nastishin, Y., Hrabchak, Z., Chernenko, A., . Buluy, O., Zelenov, P., Nazarenko, V., Kurochkin, O., & Vlokh, R. (2025). Electric field controlled switching of an optical vortex charge with a liquid crystal cell. *Optics Communications*, *579*, 131593.

Krupych, O., Adamenko, D., Dudok, T., Skab, I., Vlokh, R. (2026). Generation of the Topological Dipoles of the Orientation of Optical Indicatrix and Optical Vortices by the Bending Stress in Polycarbonate Bar**.** *Ukrainian Journal of Physical Optics*, *27*(2), 02070 – 02077.
doi: 10.3116/16091833/Ukr.J.Phys.Opt.2026.02070

Анотація. *Експериментально виявлено топологічні дефекти орієнтації оптичної індикатриси в полікарбонатному бруску, що піддається згинальному напруженню, спричиненому розподіленим навантаженням. Було виявлено, що пари топологічних дефектів формують топологічні диполі, що складаються з дефектів з однаковою напівцілою силою, але протилежними знаками. Ці топологічні дефекти генерують оптичні вихори одиничного заряду з протилежним знаком орбітального моменту імпульсу при падінні на полікарбонатний зразок циркулярно поляризованого світла. Показано, що знак орбітального моменту імпульсу вихідного променя є додатним, коли знаки сили топологічного дефекту та спінового моменту імпульсу падаючих фотонів однакові, і від'ємним, коли їх знаки різні. Отже, знак сили топологічного дефекту та спінового моменту імпульсу вхідного фотона призводить до знака орбітального моменту імпульсу, так що середовище діє на кутовий момент подібно до логічного елемента XNOR. Водночас знаки падаючого та вихідного спінових кутових моментів завжди протилежні, що відповідає логічному елементу NOT.*

Ключові слова: *топологічні дефекти, оптичний вихор, оптична індикатриса, сингулярності поляризації, згинальні напруження, полікарбонат*